Sun *et al. J Wireless Com Network (2021) 2021:132*
https://doi.org/10.1186/s13638-021-02003-4

EURASIP Journal on Wireless Communications and Networking

RESEARCH Open Access

A cable supporting test under impact loading based on 5G-IoT

Xiaokun Sun[1], Zhaohua Li[2,3] and Tao Hong[3,4*]

*Correspondence:
hongtao@buaa.edu.cn
[3] Yunnan Innovation Institute BUAA, Kunming, China
Full list of author information is available at the end of the article

Abstract

Reliable supporting effect is of utmost important for the deep mining roadway to prevent the hazards during deep mining activities. Traditional supporting equipment are not satisfying in the absence of the energy-absorbing capacity, whereas the Constant-Resistance-Large-Deformation (CRLD) cable, which can endure a large deformation of 2 m and provide a constant resistance in the meantime, would be a reasonable choice. To verify the CRLD performance of the new cable and highlight its energy-absorbing capacity under impact loading, this paper designed an in situ blasting test in a discarded deep roadway, which is divided into four sections and reinforced by the traditional and CRLD cables, respectively. Firstly, a numerical study of the blasting testis is carried out, the CRLD cable element is proposed, based on the existing one of the FLAC3D software, and a static pullout test is simulated to verify the new element, the adapted impact loading is estimated and the dynamic calculation is performed. Furthermore, under the blasting, which releases the energy of the 1st seismic magnitude, the monitored axial forces of the cables are transmitted in real time using 5G-IoT, and the supporting effects of the two types of cables are compared. According to the numerical and experimental results, the CRLD cable is proven reliable to support the deep roadway, at least shocked by the released energy corresponding to the 1st seismic magnitude.

Keywords: Energy-absorbing cable, Blasting test, 5G-IoT, Numerical analysis, Impact loading

1 Introduction

Since the beginning of the twenty-first century, enormous energy consumption and high-intensity coal mining activities have caused the depletion of shallow coal resources, which induces the sharp increase in the depth of coal mining operations [1, 2]. With increase in mining depth, the immense energy is concentred in the country rock, the country rock and the supporting system have to support not only the large crustal stress, but also the violent dynamic loading. If the support system cannot satisfy the energy-absorbing requirement, the deep mining activities will be menaced by several types of hazards, such as the coal bump [3, 4], rockbursts [5, 6], or methane emissions [7, 8]. According to previous contribution [9], roadway incidents in deep rock masses account

for 80–90% of coal mining incidents occurring in China, and the assurance of a reliable support effect for the roadway is an urgent issue in the mining engineering [10].

To solve the above-mentioned issue, numerous rock bolts/cables have been proposed. The strength bolt/cable is essentially elastic and can endure a large loading, which close to the intrinsic strength of the bolt material, they exhibit a high stiffness, while can undergo small deformations prior to failure [11], the yieldable bolt/cable presents a good ductility but a low stiffness, such as the split sets [12, 13]. However, the above-mentioned techniques cannot completely fix the issue, because the traditional equipment has no competent energy-absorbing capacity under the situation of violent energy release, and hence, a sufficient tolerance of the large deformation and a large working resistance are necessary to ensure an effective support for the deep soft rock [14]. The Constant-Resistance-Large-Deformation (CRLD) bolt, developed by He et al. [15–19], can be considered as a tested technique, which satisfying the above-mentioned requirements. Based on the CRLD bolt, the CRLD cable was then developed, which could endure the large deformation of 2 min laboratory tests [20], and had been widely used in several real projects for the slope reinforcement and monitoring [21]. The CRLD cable is composed of a rigid cone, a steel pipe, and a cluster of strands, as shown in Fig. 1. One end of the strands is forged with the cone, the other end is fixed together using a nut, the pipe is anchored into country rock using grout, and the tolerance of large deformation and constant resistance are made possible by the relative sliding of cone-pipe when the tensile loading is exerted on the strands. The mechanical performance of the CRLD cable under the static loading has been systematically studied according to many laboratory tests [20] and real projects applications [21]; however, the dynamic loading is usually dominant during the deep mining activities, for example, the coal bump.

This paper is thus focused on the comparison of the supporting effects between the traditional and CRLD cable under the impact loading. The numerical simulation towards a deep mining roadway and the corresponding in situ blasting test are performed to compare the performance of the two types of cables. As the latest breakthrough in communication field, the fifth-generation (5G) mobile network and Internet of Things (IoT) technology have present significant potential to get and transmit data in high speed and high quality [22–24], this paper also attempted to transmit the monitored axial forces via the high-speed wireless networks in in situ test in order to ensure the data transmission effect under the blasting condition.

This paper is organized as follows: In Sect. 2, the geological conditions of the test location and the monitoring equipment based on 5G-IoT and the blasting test are presented;

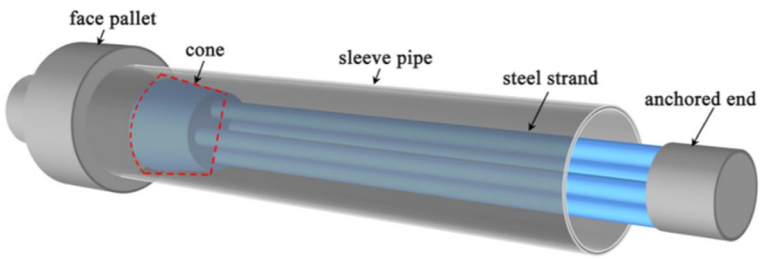

Fig. 1 Components of the CRLD cable in three-dimensional view [21]

in Sect. 3, the corresponding numerical model are detailed; in Sect. 4, the experimental results are given, and then they are compared with the numerical ones; Sect. 5 is devoted to give some conclusions.

2 Methods/experimental

2.1 Geological background and site details

The blasting test was performed in a discarded mining roadway located in the Hongyang 3rd mine, whose maximum mining depth exceeded 1000 m. With the increase of the mining depth, because of the complex geological structure and the larger and larger crustal stress, the coal bumps occurred nearby frequently. As shown in Fig. 2a, the 1213 connection roadway this paper studied was located in the 1st of northern mining area, with a depth of 770–793 m, an average inclination of 6°, and a total length of 303 m. The geological condition was relatively simple around this roadway, neither subsided column nor fault was observed, and the lithology of the country rock was regular, the lithology and the thicknesses of the country rocks are shown in Fig. 2b.

2.2 Supporting system in the test section

Along the 1213 connection roadway, a section of 40 m was chosen for the blasting test, and then it was divided into four segments with a length of 10 m, respectively, as shown in Fig. 3a. As the objective of this test is to compare the supporting effects of traditional and CRLD cables under the same geological and initial supporting conditions, so the traditional cables were kept in section I and IV, the CRLD cables were installed in section II and III. The rectangle roadway presented a section of 4.0 m × 2.5 m, and was supported by the bolt-mesh-cable system before the blasting test was carried out. The distribution of the supports on the roof shown in Fig. 3b–d gives the dimension of cross sections I and II, respectively, and the distribution of the supports (the blue lines stand for the cables, and the black denote the bolts). The monitoring point was set in the cables on the sidewall, as shown in Fig. 3c. The geometric and physical parameters for all the cables are identical, both the tradition and CRLD cables had the same tensile strength of 650 kN, and the tolerance of the deformation and the constant resistance of the CRLD cable

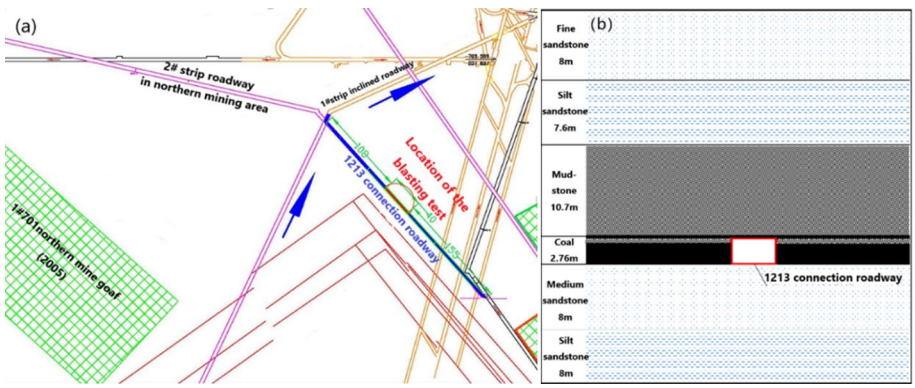

Fig. 2 Location and geological condition of the test site: **a** roadway location where the blasting test was performed; **b** lithology of the country rocks

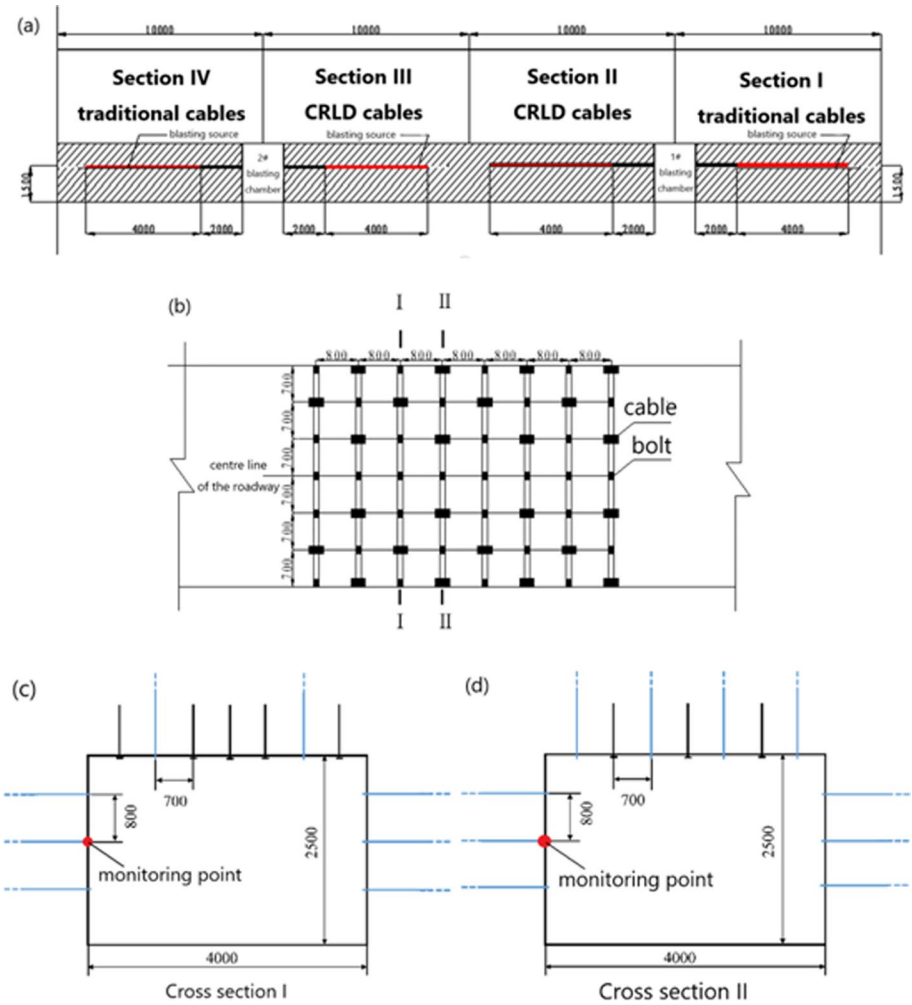

Fig. 3 Division and supporting system of the test roadway (the blue lines denote the cables, and the black lines the bolts): **a** Four sections of the test roadway and location of the blasting sources; **b** supporting system on the roof of the test roadway; **c** cross section I, and **d** cross section II

Table 1 Geometrical and mechanical parameters of bolts and cables

	Tensile strength (kN)	Young's Modulus (GPa)	Diameter (m)	Length (m)	Pre-tightening force (kN)	Cross section (m^2)	Constant resistance (kN)	Tolerant deformation (mm)
CRLD cable	650	205	0.068138	6.5	300	3.7e−4	350	650
Traditional cable	650	205	0.068138	6.5	300	3.7e−4	–	–
Traditional bolt	100	205	0.0628	4	0	3.14e−4	–	–

are 650 mm and 350 kN, respectively, and the initial pre-tightening force of 300 kN was exerted for all of the cables. The corresponding parameters are listed in Table 1.

2.3 Monitoring equipment based on 5G and IoT

In scientific experiments and industrial production, high-quality and real-time data transmission is often necessary. As the latest breakthrough in communication field, 5G has present many advantages such as high speed, large capacity and low latency. In 5G networks, a multi-layer structure will be considered owing to the heterogeneity of the equipment and services. Regarding the IoT, it is a potential technology to realize the interconnection of all things, the popularity of small and inexpensive computing devices with sensing and communication functions is paving the way for the widespread application of IoT [25]. In particular, many IoT terminal devices will play an important role in 5G communication system, such as autonomous driving or a surveillance system with a high-definition camera. In this in situ test, the corresponding IoT terminals are used to monitor the axial forces of cables in real time, and in order to reduce the data transmission delay, 5G communication channels are chosen to transmit data.

The monitoring system that monitoring the axial forces and deformations of the cables during the test is shown in Fig. 4, which is composed of the sensors, the data collecting instrument, the charge conditioner and the computer. The data collecting instrument plays a central role in the entire system, it supplies power to the sensors through the charge conditioner; in order to ensure the data transmission effect under

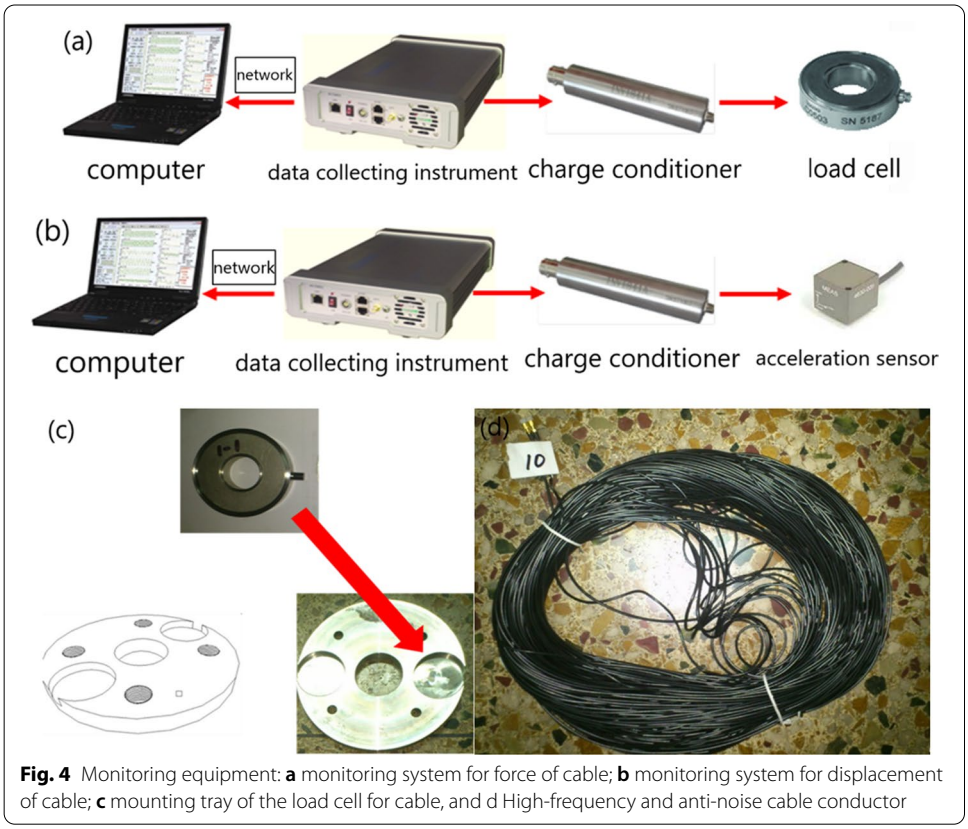

Fig. 4 Monitoring equipment: **a** monitoring system for force of cable; **b** monitoring system for displacement of cable; **c** mounting tray of the load cell for cable, and d High-frequency and anti-noise cable conductor

the blasting condition, the high-frequency and anti-noise cable conductors were used to transmit signals between sensors and the data collecting instrument. Next, the data collecting instrument uses the 5G wireless interface to transmit signals to the outside, as shown in Fig. 4d.

3 Numerical analysis

3.1 Numerical model

According to the geological condition shown in Fig. 2b, the numerical model of the test section was established usingFLAC3D software, as shown in Fig. 5a. To ensure the calculation accuracy and avoid boundary effect, the dimension of the model was set as 54 m × 40 m × 45 m. The model is perpendicularly restrained on the 4 lateral faces. The three-direction displacement is constraint at the bottom of the numerical model, whereas the top face is free. The viscous boundary conditions are assigned in global model, and it should be noted that the free-field boundary is not necessary, in case that the dynamic sources are within the model [26]. The country rocks were described using the perfect elastic–plastic model, incorporating the Mohr–Coulomb plastic limit criterion [26]. The physical and mechanical parameters that used in the study were determined by laboratory tests of the corresponding rock samples, and were enumerated in Table 2. The depth of the studied roadway is about 770–793 m, so the corresponding gravity initialization was carried out before the dynamic loading was exerted. The

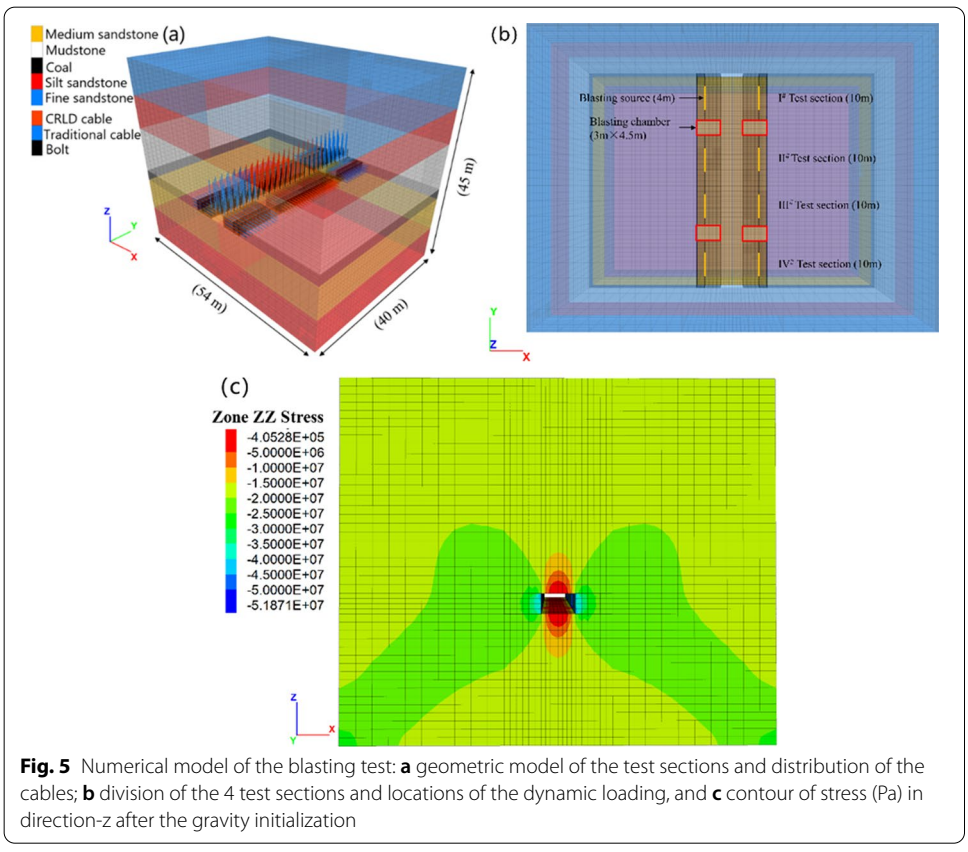

Fig. 5 Numerical model of the blasting test: **a** geometric model of the test sections and distribution of the cables; **b** division of the 4 test sections and locations of the dynamic loading, and **c** contour of stress (Pa) in direction-z after the gravity initialization

Table 2 Physical–mechanical parameters of adjoining rocks

	Density (Kg/m^3)	Young's modulus (GPa)	Poisson's ratio	Tensile strength (MPa)	Cohesion (MPa)	Friction angle (°)
Coal	1400	1.0	0.36	1.15	13.0	21.4
Mudstone	2300	20	0.35	2.5	21.6	36.0
Siltstone	2590	40	0.23	3.0	50.0	35.0
Fine sandstone	2800	35	0.22	2.98	52.0	33.0
Medium sandstone	2630	40.9	0.2	3.08	45.0	38.0

contour of the stress in vertical direction is shown in Fig. 5c, and the initial stress is about 10–35 MPa.

3.2 Static pullout test of the CRLD and traditional cables

The cables and bolts were installed in the numerical model, and were completely in line with the above-mentioned system model: Sections I and IV were reinforced by traditional cables and bolts, whereas sections II and III were reinforced by CRLD cables and traditional bolts. According to the mechanical performance of the CRLD cable [20] and the existing cable element of the FLAC3D software [26], the CRLD cable element was developed. A tension-deformation relationship, which describing the large deformation and constant resistance performance of CRLD cable, is proposed in Eq. (1).

$$F = \begin{cases} KU(F \leqslant F_{CR}) \\ F_{CR}(F > F_{CR}, U \leqslant U_M) \\ KU(F_{CR}\langle F \leqslant F_S, \ \ U\rangle U_M) \\ 0(F > F_S) \end{cases} \tag{1}$$

In case that the load F on the CRLD cable is smaller than the constant resistance F_{CR}, the tension–deformation relation is elastic, as $F=KU$, where K is the cable rigidity and U is the axial deformation; in case that F is greater than F_{CR} and U is smaller than the tolerant deformation U_M, the tensile strength F_S is set to be F_{CR}, to remain the tensile force with a value of F_{CR}; in case that F is less than F_S and U is larger than U_M, F_S is set to be the initial tensile strength, so the tension-deformation relation represents the elastic behavior, as $F=KU$; in case that F continues to increase and reach the tensile strength, F_S is assigned to vanish, and it means the failure of the CRLD cable.

To validate the performance of CRLD cable element, a static pullout test was carried out using FLAC3D software, and a performance comparison between CRLD cable and the traditional one was presented. The involved physical and mechanical parameters of the cables were used in line with Table 1. As shown in Fig. 6a, one end of the cable was fixed, another end was loaded with a constant velocity $V=20$ mm/min. Under the quasi-static loading, the traditional cable will fail once the axial tension reach the tensile strength 650 kN, and its axial deformation was limited within a small value; however, after the tensile loading reaches the constant force 350 kN, the CRLD cable will present a good ductility, and the tolerant deformation was 650 mm (see Fig. 6b).

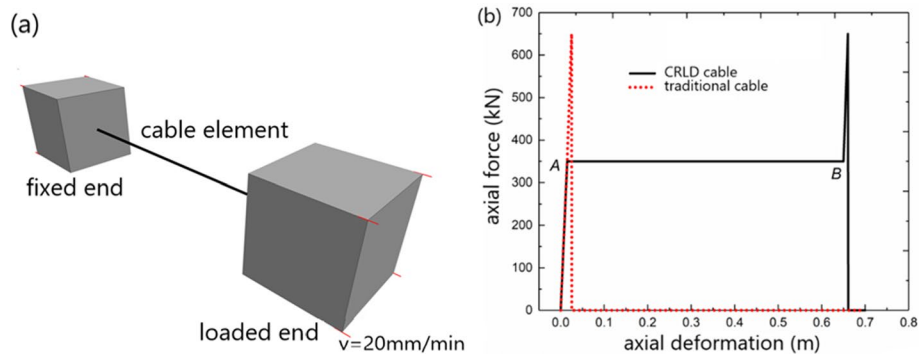

Fig. 6 Static pullout tests of the traditional and CRLD cables: **a** numerical model of the static pullout test, and **b** comparison of the numerical results

Table 3 The statistics of impact loading caused by mine seismicity [29]

	Released energy	Frequency/Hz	Amplitude(velocity)/(m/s)	Strain rate/(s^{-1})
1	296	5–30	0.13–0.40	1.6×10^{-3} to 3.0×10^{-2}
2	400	5–30	0.18–0.40	2.3×10^{-3} to 5.0×10^{-2}
3	895	3–28	0.20–0.65	1.5×10^{-3} to 4.6×10^{-2}
4	1240	3–25	0.20–0.84	1.5×10^{-3} to 5.3×10^{-2}
5	8270	2–18	0.34–1.00	1.7×10^{-3} to 4.6×10^{-2}
6	22,600	2–18	0.79–3.44	4.0×10^{-3} to 1.6×10^{-1}
7	27,100	1–15	0.44–3.50	1.1×10^{-3} to 1.3×10^{-1}
8	50,400	2.5–15	0.50–3.27	3.2×10^{-3} to 1.2×10^{-1}
9	103,000	0.5–12	1.23–3.65	1.6×10^{-3} to 1.1×10^{-1}
10	3,970,000	0.4–5	8.45–12.27	8.6×10^{-3} to 1.6×10^{-1}

3.3 Dynamic loading

According to the simple harmonic waves based on seismic wave theory [27, 28], the in situ wave data is considered as a function of the seismic source, the rock medium, and the seismic recording system. Hence, it is difficult to obtain the accurate vibration velocity history signals of a medium that near the seismic source [29]. In this study, the following wave equation [29] was used to simulate the impact loading, whose released energy was equivalent to the 1st seismic magnitude.

$$A(t)=\begin{cases}\frac{1}{2}A_0\left[1-\cos\left(\frac{2\pi t}{\tau}\right)\right] & t_0<t<\tau+t_0\\ 0 & t\langle t_0,\ t\rangle\tau+t_0\end{cases} \tag{2}$$

where A_o is the amplitude of the impulse, τ is the duration of the impulse, $f=l/\tau$ is the frequency, and t_0 is the start time of the impulse. Many in situ measurements of dynamic

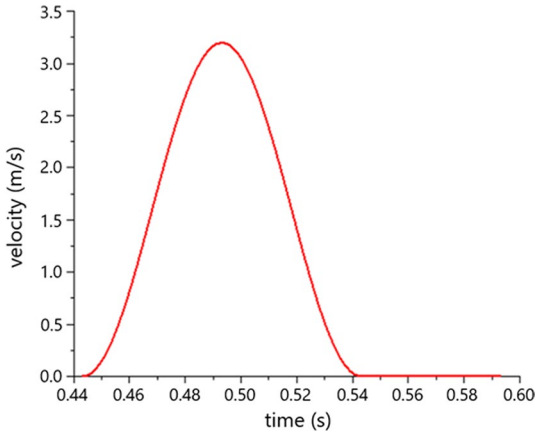

Fig. 7 Input wave curve corresponding to the released energy of the 1st seismic magnitude

loading, induced by mine seismicity or coal bump, are summarized in Table 3, and these values can be used to determine the input parameters of the dynamic loading [29]. In this study, the data that corresponding to the released energy of 103,000 J in Table 3 (1st seismic magnitude) were used. Introducing the frequency of 10 Hz, and the amplitude of 3.25 m/s, the input impact wave is shown in Fig. 7. The dynamic loading was thus exerted to the interior grid points in form of velocity history in accordance with Fig. 5b.

For the dynamic analysis in the framework of FLAC3D software, local damping, Rayleigh damping and hysteretic damping are common coefficients that used for the energy dissipation [26]. Wang compared the effects of Rayleigh damping and local damping in a dynamic calculation for coal pillars, and observed the similar results [29]. Compared with Rayleigh damping, local damping gives acceptable result for simple cases due to its frequency-independence, and it is not necessary to estimate the natural frequency of the studied system with local damping. Hence, the local damping is used in this study, with the local damping coefficient α_L determined by Eq. (3), as follows:

$$\alpha_L = \pi D \tag{3}$$

Where D is a fraction of the critical damping, which 5% is a typical value for dynamic analysis, and α_L is thus equal to 0.157 in this study.

4 Results

4.1 In situ blasting test based on 5G-IoT

The impact wave is generally induced by the elastic energy release, which can come from mechanical vibration, blasting, strata caving, fault slip, and other causes [30, 31]. In deep mining engineering, coal bump, rock burst, or micro-seismicity may be the triggering events, and the damage against rock and supporting system is similar to the blasting, which corresponds to the quick transformation of the chemical energy to the impact wave of high pressure air. By controlling the charge quantity of explosive, it is possible to simulate the impact wave and to observe its consequence by using the blasting test. In this study, the blasting whose releasing energy is corresponding to the 1st seismic

magnitude was carried out, and the supporting effects of the traditional and CRLD cables were compared.

4.2 Blasting program

In order to simulate the impact effect of the blasting against the country rock and the supporting system, the blasting sources were placed behind the sidewalls, parallel to the strike of the roadway. As shown in Fig. 3a, several blasting caves were excavated between the sections I and II, and III and IV, with a section of 3 m × 2.5 m and a length of 4.5 m.

This test carried out a blasting with a released energy of about 1×10^5 J, corresponding to the1st seismic magnitude. The emulsion explosive of 1.2×10^4 J/kg was used, and the corresponding charge quantity was 8.5 kg, taking into account the energy dissipation during the test, the charge quantity of 10 kg was considered. The load cells were firstly installed, and then the mounting tray. After the pre-tightening force was loaded, the signal transmitting devices were installed, and the signal transmission lines were laid.

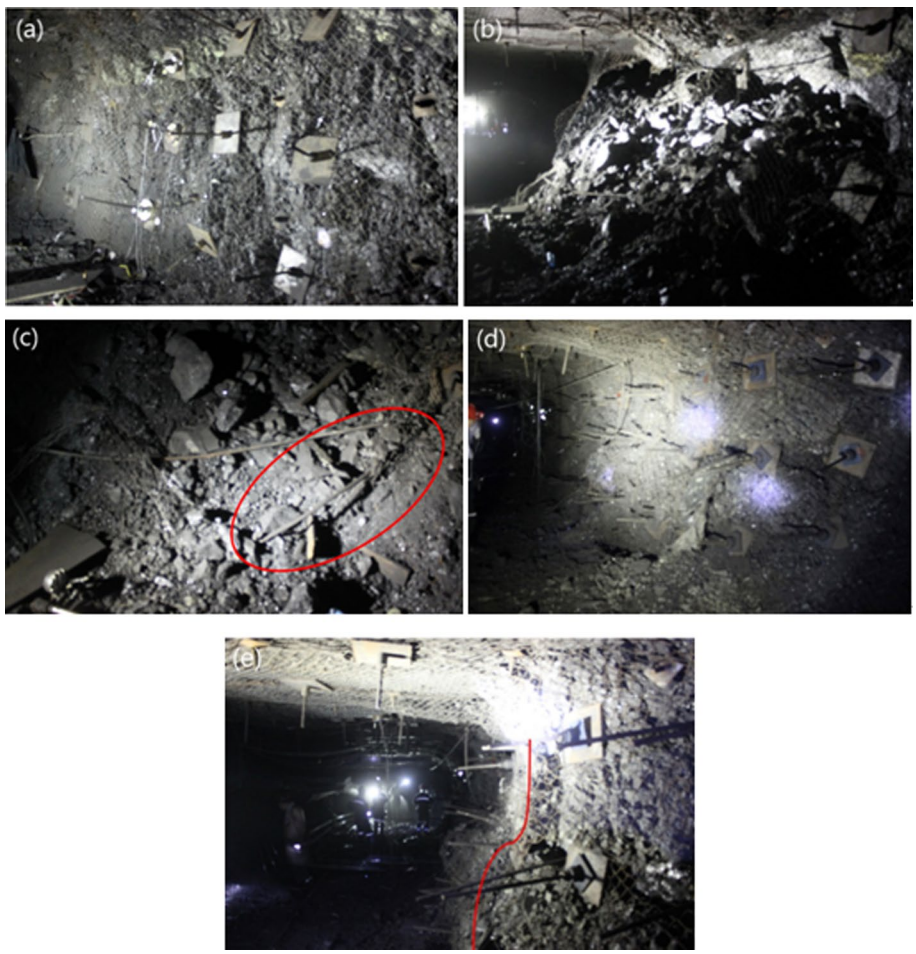

Fig. 8 Supporting effects of the traditional and CRLD cables: **a** sidewall supported by traditional cables before the blasting; **b** sidewall supported by traditional cables after the blasting; **c** traditional cable pulled out due to the blasting; **d** sidewall supported by CRLD cables before the blasting, and **e** sidewall supported by CRLD cables after the blasting

4.3 In situ observation results

Figure 8 gives the comparison of the roadway before and after the blasting. According to Fig. 8a, the roadway reinforced by the traditional cables (section I) was stable before the blasting, after the blasting, the country rock was globally instable, and the sidewall collapsed completely (see Fig. 8b), some cables were pulled out (see Fig. 8c), and almost all the cables failed. According to the observation in the field, the deformations of the rock and the traditional cables are not coordinated, thus the collapsed rock degraded the anchorage effect of the cables, so the traditional cables cannot restrain the deformation of the country rock effectively. According to Fig. 8d, the roadway supported by the CRLD cables (section II) was stable before the blasting, after the blasting, no wall caving appeared, only a large deformation with a maximum value of 300 mm is observed from the bottom up to 1 m, and the roadway globally remained stable.

As a conclusion, under the same geological condition and the same impact energy, the roadway reinforced by the traditional cables collapsed, whereas that by the CRLD cables only presented controllable deformation within same zones. The reliable ductility of the latter made it possible to absorb the energy released by the blasting, and the constant resistance during the large deformation stage restrains the further deformation of the country rock.

5 Discussion

5.1 Test data analysis

Under the impact loading that corresponding to the 1st seismic magnitude, the axial forces of the cables are presented in Fig. 9. There into, the red and black lines denote the monitoring data in the field and the numerical result, respectively. Figure 9a gives the axial force of the traditional cable, and an acceptable agreement of the monitoring and numerical data is observed except some oscillations of the monitoring data. Once the axial force reaches the tensile strength (650 kN), it vanishes sharply, and the traditional cables fail within 0.01 min. According to Fig. 9b, the axial force of the CRLD cable reaches the constant resistance (350 kN), the axial force is limited within the constant resistance, because the large deformation occurs during the impact loading, and the released energy is absorbed. After some oscillations, the axial force remains to a value

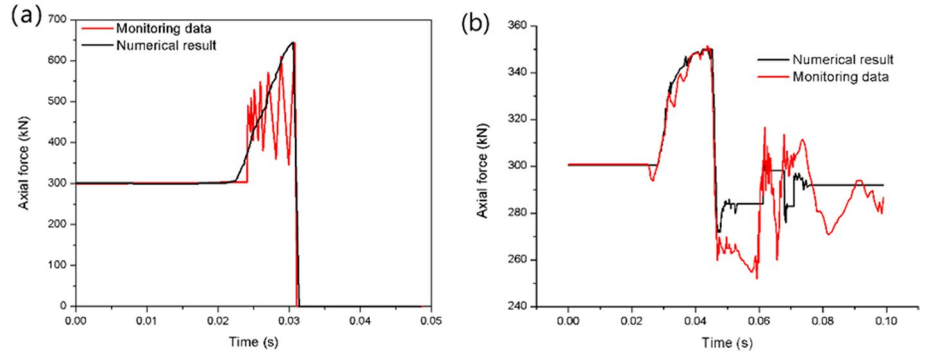

Fig. 9 Numerical and experimental results of the axial force evolutions of traditional and CRLD cables under impact loading: **a** numerical and experimental results of the axial force evolutions of the traditional cable, and **b** numerical and experimental results of the axial force evolutions of the CRLD cable

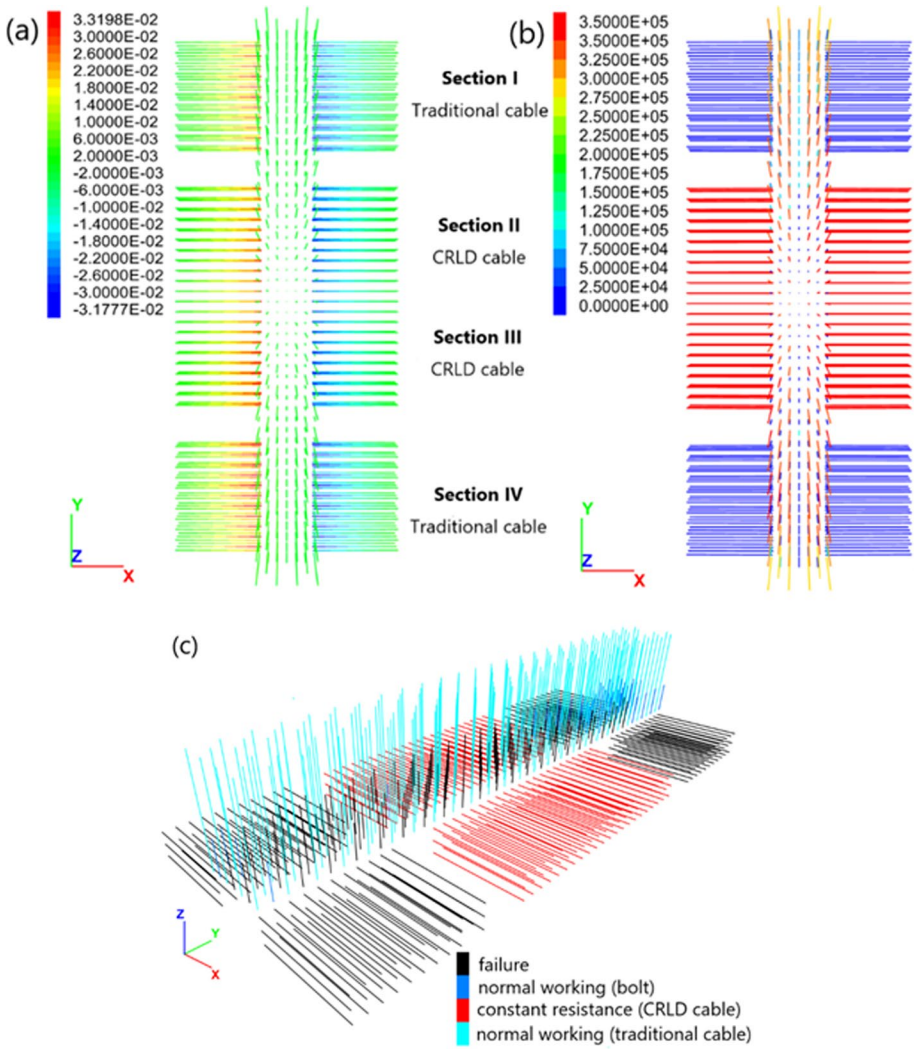

Fig. 10 Axial deformations, axial forces and working conditions of the traditional and CRLD cables after the impact loading: **a** axial deformations of the traditional and CRLD cables after the impact loading; **b** axial forces of the traditional and CRLD cables after the impact loading, and **c** working conditions of the traditional and CRLD cables after the impact loading

of 280–290 kN, which is smaller than the initial value (300 kN), it means that the crustal stress decreases due to the released energy.

Figure 10a presents the axial deformations of all the cables after the blasting, with the same impact loading, the deformations of the traditional and CRLD cables are similar, and the maximum value is about 30 mm. According to Fig. 10b, the axial forces of the traditional cables in section I and IV have decreased to 0, while those of the CRLD cables are 300–350 kN with a large deformation of about 30 mm. Finally, Fig. 10c gives the working states of the cables. All the traditional cables on sidewall have failed, while the CRLD cables still work.

6 Conclusion

To ensure the stability of the deep mining roadway, the reliable supporting device with a tested energy-absorbing performance is necessary. In this paper, the recently-developed CRLD cable is briefly presented, in addition, the CRLD cable element was proposed within the framework of the FLAC3D software, and the static pull-out test was performed to verify its energy-absorbing capacity in numerical approach. Furthermore, the numerical model of the blasting test was established and the dynamic calculation was performed.

Then, in the in situ test, a blasting test whose released energy is equivalent to that of the first seismic magnitude is performed in a discarded deep roadway to verify the performance of CRLD cable, and the monitored axial forces are transmitted via 5G-IoT which present an excellent robustness. Then, the supporting effects of the CRLD and traditional cables are compared, under the same geological and dynamic loading conditions. According to the in situ test, the test section reinforced by the traditional cables were completely collapsed after the blasting, and almost all cables were failed, whereas that reinforced by the CRLD cables remained a globally stable state, and all the CRLD cables kept a normal working condition. An acceptable agreement of the monitoring and numerical data was observed except some oscillations of the monitoring data, and the better ductility of the CRLD was proven.

As conclusion, most of the traditional cables failed immediately under the impact loading, but the CRLD cable exhibited a good energy-absorbing performance. The reliable ductility and sufficiently large stiffness of the CRLD cable make it possible to absorb the energy released by the blasting, and the constant resistance during the large deformation stage restrains the further deformation of the country rock. In addition, 5G-IoT technology is also proven reliable to transmit monitored data in blasting tests.

Abbreviations

CRLD cable: Constant-Resistance-Large-Deformation cable; IoT: Internet of things; 5G: Fifth generation.

Authors' contributions

XS and TH discussed and conceived the research, XS wrote the manuscript, ZL performed the numerical analysis, TH conducted the data communication in the field test and revised the article. All authors read and approved the final manuscript.

Funding

No funding was received during this work.

Availability of data and materials

Data sharing not applicable to this article as no datasets were generated or analyzed during the current study.

Declarations

Competing interest

This work has not been previously published or it won't be submitted to another journal for publication. This work is original and does not infringe upon any existing or third party copyrights. All authors hereby transfer all rights under copyright to the EURASIP Journal on Wireless Communications and Networking. For this work that is jointly authored, the corresponding author signs as the authorized agent for all concerned.

Author details

[1]School of Mechanics and Civil Engineering, China University of Mining and Technology (Beijing), Beijing 100083, China. [2]Department of Civil Engineering, Yango University, Fuzhou 350015, China. [3]Yunnan Innovation Institute BUAA, Kunming, China. [4]School of Electronics and Information Engineering, Beihang University, Beijing, China.

Received: 4 December 2020 Accepted: 12 May 2021
Published online: 26 May 2021

References

1. C.L. Wang, G.Y. Li, A.S. Gao, F. Shi, Z.J. Lu, H. Lu, Optimal pre-conditioning and support designs of floor heaven in deep roadways. Geomech. Eng. **14**(5), 429–437 (2018)
2. C.L. Wang, X.S. Chuai, F. Shi, A.S. Gao, T.C. Bao, Experimental investigation of predicting rockburst using Bayesian model. Geomech. Eng. **15**(6), 1153–1160 (2018)
3. A. Diaz, B. Maria, C. Gonzalez, Influence of the stress state in a coal bump-prone deep coalbed: a case study. Int. J. Rock Mech. Min. Sci. **46**(2), 333–345 (2009)
4. K. Holub, J. Rušajová, J. Holečko, Particle velocity generated by rockburst during exploitation of the longwall and its impact on the workings. Int. J. Rock Mech. Min. Sci. **48**, 942–949 (2011)
5. P. Konicek, J. Schreiber, Rockburst prevention via distress blasting of competent roof rocks in hard coal longwall mining. J. South Afr. Inst. Min. Metall. **118**(3), 235–242 (2018)
6. L. Wojtecki, M.J. Mendecki, W.M. Zuberek, Determination of destress blasting effectiveness using seismic source parameters. Rock Mech. Rock Eng. **50**(12), 3222–3244 (2017)
7. E. Krause, Short-term predictions of methane emissions during longwall mining. Achieves Min. Sci. **60**(2), 581–594 (2015)
8. D. Qian, H. Shimada, Z. Zhang, T. Sasaoka, K. Matsui, Application of goaf-side roadway retained and new type ventilation system in deep longwall face. Mem. Fac. Eng. Kyushu Univ. **74**(3), 99–116 (2015)
9. Z.H. Li, Z.G. Tao, Z.G. Meng, M.C. He, Longwall mining method with roof-cutting unloading and numerical investigation of ground pressure and roof stability. Arab. J. Geosci. **11**, 1–13 (2018)
10. X.S. Liu, J.G. Ning, Y.L. Tan, Q. Xu, D.Y. Fan, Coordinated supporting method of gob-side entry retaining in coal mines and a case study with hard roof. Geomech. Eng. **15**(6), 1173–1182 (2018)
11. C.C. Li, A new energy-absorbing bolt for rock support in high stress rock mass. Int. J. Rock Mech. Min. Sci. **47**, 396–404 (2010)
12. T.F. Herbst. Yieldable roof support for mines. *in: Proceedings of the 31st US Symposium. Rotterdam and Brookfield*, pp. 807–814 (1990).
13. W.D. Ortlepp, Yieldable rock bolts for shock loading and grouted bolts for faster rock stabilization. Mines Maga, ColoSch Mines **60**(3), 12–17 (1970)
14. A. Ansell, Laboratory testing of a new type of energy absorbing rock bolt. Tunn. Undergr. Space Technol. **20**(4), 291–330 (2005)
15. M.C. He, W.L. Gong, J. Wang et al., Development of a novel energy-absorbing bolt with extraordinarily large elongation and constant resistance. Int. J. Rock Mech. Min. Sci. **67**(1), 29–42 (2014)
16. Z.H. Li, J. Hu, H.X. Zhu, J.L. Feng, M.C. He, Numerical study on the CRLD cable–rock interaction under static pull-out loading using coupled DEM–FDM method. Acta Geotechnica **15**(8), 2137–2158 (2020)
17. Z. Li, Q. Lv, H. Zhu, J. Hu, J. Feng, M. He, Laboratory testing and modeling of a high-displacement cable bolt. Int. J. Geomech. **19**(7), 04019078 (2019)
18. J. Hu, Z. Li, F. Darve, J. Feng, Advantages of second-order work as a rational safety factor and stability analysis of a reinforced rock slope. Can. Geotech. J. **57**(5), 661–672 (2020)
19. Z. Li, Z. Tao, Y. Jiang, Q. Lv, F. Darve, M. He, Real-time monitoring and FEMLIP simulation of a rainfall-induced rockslide. Nat. Hazards Earth Syst. Sci. **19**(1), 153–168 (2019)
20. X.M. Sun, Y. Zhang, D. Wang et al., Mechanical properties and supporting effect of CRLD bolts under static pull test conditions. Int. J. Miner. Metall. Mater. **24**(1), 1–9 (2017)
21. Z.H. Li, Y.J. Jiang, Z.G. Tao et al., Monitoring prediction of a rockslide in an open-pit mine and numerical analysis using a material instability criterion. Bull. Eng. Geol. Env. **2**, 1–13 (2018)
22. S. Sun, M. Kadoch, L. Gong, B. Rong, Integrating network function virtualization with SDR and SDN for 4G/5G networks. IEEE Netw. **29**(3), 54–59 (2015)
23. Y. Wu, B. Rong, K. Salehian, G. Gagnon, Cloud transmission: a new spectrum-reuse friendly digital terrestrial broadcasting transmission system. IEEE Trans. Broadcast. **58**(3), 329–337 (2012)
24. N. Zhang, N. Cheng, A.T. Gamage, K. Zhang, J.W. Mark, X. Shen, Cloud assisted HetNets toward 5G wireless networks. IEEE Commun. Mag. **53**(6), 59–65 (2015)
25. B. Rong, Y. Qian, K. Lu, H. Chen, M. Guizani, Call admission control optimization in WiMAX network. IEEE Trans. Veh. Technol. **57**(4), 2509–2522 (2008)
26. Itasca. FLAC3D User Manual, Version 6.0. Itasca Consulting Group Inc., USA (2012)
27. M.S. Gao. Study on the strong-soft-strong structure control mechanism of roadway subjected to rock burst. Ph.D. thesis. Jiangsu: China Univ Min Tech, Xuzhou (2006).
28. S. Zarnani, M.M. El-Emam, R.J. Bathurst, Comparison of numerical and analytical solutions for reinforced soil wall shaking table tests. Geomech. Eng. **3**(4), 291–341 (2011)
29. S.L. Wang, S.P. Hao, Y. Chen et al., Numerical investigation of coal pillar failure under simultaneous static and dynamic loading. Int. J. Rock Mech. Min. Sci. **84**, 59–68 (2016)
30. V.A. Mansurov, Prediction of rockbursts by analysis of induced seismicity data. Int. J. Rock Mech. Min. Sci. **38**, 893–901 (2001)
31. A. McGarr, Energy budgets of mining-induced earthquakes and their interaction with nearby stopes. Int. J. Rock Mech. Min. Sci. **37**, 437–443 (2000)

Publisher's Note